Scientific Research Journal,
Vol 17, No 2 (2020) 149-162
https://doi.org/10.24191/srj.v17i2.9918

First-Principles Study on Structural and Electronic Properties of Cubic (Pm3m) And Tetragonal (P4mm) $ATiO_3$ (A=Pb, Sn)

N.N. Alam[1,5], N.A. Malik[1,5], M.H. Samat[5], M.Z. Mohyedin[1, 5], N.H. Hussin[2], A.M.M. Ali[1,5],O.H. Hassan[3,5], M.Z.A. Yahya[4,5], M.F.M. Taib[1,5*]

[1]Faculty of Applied Sciences, Universiti Teknologi MARA, 40450 Shah Alam, Selangor, Malaysia
[2]Faculty of Applied Sciences, Universiti Teknologi MARA, 26400 Jengka, Pahang, Malaysia
[3]Faculty of Arts and Design, Universiti Teknologi MARA, 40450 Shah Alam, Selangor, Malaysia
[4]Faculty of Defence Science & Technology, Universiti Pertahanan Nasional Malaysia, 57100 Kuala Lumpur, Malaysia
[5]Ionic Materials and Devices (iMADE), Institute of Science, Universiti Teknologi MARA, 40450 Shah Alam, Selangor, Malaysia

**Corresponding author's e-mail: mfariz@uitm.edu.my*

Received: 21 Jan 2020
Accepted: 13 August 2020
Online First: 25 August 2020

ABSTRACT

This work focuses on exploring lead-free ferroelectric materials that have a comparable unique ns^2 solitary pair electrons with Pb (II), for example, Sn (II) using the first-principles study. All counts were performed dependent on ultrasoft pseudopotential of Density Functional Theory (DFT) that has been executed in the Cambridge Serial Total Energy Package (CASTEP). The convergence test for cut-off energy and k-point was performed to measure the accuracy of the calculations. It is shown that the structures have threshold energy of 350 eV and k-point of 4x4x4 with Monkhorst Pack. The structural properties for both cubic and tetragonal structures $ATiO_3$ (Pb, Sn) have shown the comparable value of the lattice parameter that was in agreement with previous work. Generalised gradient approximation (GGA) PBE displays the most exact qualities for cross-section parameters concerning exploratory qualities for both cubic $PbTiO_3$ while GGA-PBEsol functional is the best functional approximation for tetragonal PTO. The

Copyright© 2020 UiTM Press.
This is an open access article
under the CC BY-NC-ND license

electronic band structure and density of states show the presence of hybridizations between anion O 2p and cation Pb 6s/Sn 5s unique solitary pair in tetragonal PTO and SnTO stage. The calculations have shown that both cubic and tetragonal structure of $ATiO_3$ (A=Pb, Sn) has an indirect bandgap of 1.169 eV, 1.164 eV, 1.703 eV, and 1.016 eV respectively. It is shown that tetragonal structures have a higher value of bandgap compared to cubic structures.

Keywords: *density functional theory; electronic properties; $PbTiO_3$; $SnTiO_3$*

INTRODUCTION

Ferroelectrics are pyroelectric as they can initiate transitory voltage when they are warmed or cooled [1,2]. One of the best ferroelectric materials is perovskite oxide, which has a general chemical formula of ABO_3 [3]. Perovskite oxide will change its phase from tetragonal (P4mm) to cubic (Pm3m) at 800K [4,5]. Example of perovskites such as $PbTiO_3$ and $SnTiO_3$. $PbTiO_3$ is widely used as piezoelectric sensors due to its high photorefractive sensitivity, memory, computer random-access memory (RAM), and radio-frequency identification (RFID) cards [6,7]. $PbTiO_3$ possess high spontaneous polarisation and dielectric constant of 0.75 C/m^2 and 1.767 $x10^{-2}$ S/cm respectively [8]. However, since Pb is high in toxicity, it will increase air pollution and affect the environment [9]. A portion of the destructive impacts of Pb on a person can cause cerebral pain, a sleeping disorder, and cause forceful conduct [10]. It is profoundly required to supplant it with natural inviting and elite lead-free ferroelectric materials [11]. $SnTiO_3$ is anticipated to have a huge closeness with $PbTiO_3$ as Sn is in a similar group with Pb [12]. It also has higher spontaneous polarisation (1.1 C/m^2) than Pb, indicating it as a good candidate to replace Pb [13]. Many researchers suggested $SnTiO_3$ is most likely suitable to reduce the consumption of Pb, creates a healthy and safe environment for the surrounding. Be that as it may, $SnTiO_3$ is not yet synthesis. A stable ferroelectric structure has been reported; however, there is no analysis of the electric polarisation [14]. Other than that, the strength of $PbTiO_3$ and $SnTiO_3$ are as yet vague [15]. 2It is hard to prepare a single period of $SnTiO_3$ due to the disproportional of Sn^{2+} at high temperatures [16]. In this study, the structural and electronic properties of $PbTiO_3$ and $SnTiO_3$ are identified. Subsequently, the first-principles study

is used to investigate the electronic properties, phase stability, and strain properties of $PbTiO_3$ and $SnTiO_3$. DFT can be dictated by computing the energy of the ground state, which comprises kinetic energy and potential energy [17].

Computational Method

In this work, cubic (paraelectric, Pm3m) and tetragonal (polar, P4mm) ATiO3 (A=Pb, Sn) were investigated by using DFT CASTEP computer code [18]. Convergence tests were carried out with convergence of energy change per atom $<5\times10^{-6}$ eV, residual force <0.01 eV/Å, stress <0.02 GPa, and displacement of atoms <0.0005 Å [19]. The k-point used for each compound of PTO and SnTO for both cubic and tetragonal structures was 4x4x4 with 350 eV cut-off energy Monkhorst Pack [20]. GGA-PBE and GGA-PBEsol were utilised for cubic and tetragonal structures $ATiO_3$ (A=Pb, Sn), respectively [21]. Consequently, it very well may be noticed that the extraordinary point connected for Brillouin zone cubic structure inspecting for all compounds ought to be set with a similar k-point (4x4x4) in light of their comparative space group [22]. The electronic properties, which consist of band structure and density of state (DOS), were calculated by using ultrasoft pseudopotential [23].

RESULTS AND DISCUSSION

Geometrical Optimisation

Figure 1 shows the cubic and tetragonal structures for $ATiO_3$. The estimations of structural cross-section parameters for PTO and SnTO LDA, GGA-PBE, and GGA-PBEsol functionals DFT are shown in Table 1 for cubic structure and Table 2 for tetragonal structure, respectively. The precision of the cross-section computation is significant because the difference in 1-2% of the grid will influence the unsteadiness of perovskite oxide. The test is fundamental to be completed to distinguish the best functional that would be implemented to different computations of new materials SnTO. The relative

deviations are overestimated 1.71% for LDA-CA-PZ, belittled 0.33% for GGA-PBE, and overestimated 0.78 % for GGA-PBEsol when contrasted with the experiment of PTO (3.96 Å). The geometrical optimisation shows that GGA-PBE gives the best approximation with a percentage difference of less than 1%. Results, as organised in Table 2, show that each functional LDA-CAPZ and GGA-PBE for the tetragonal PTO gives more significant deviations in computing lattice parameter and volume. The lattice parameter utilising the GGA-PBEsol is extremely near the experimental value, with just a deviation of 0.01%. This outcome is superior to anything than that of the determined outcomes utilising LDA-CAPZ and GGA-PBE with a deviation of +2.16% and -7.27%, respectively.

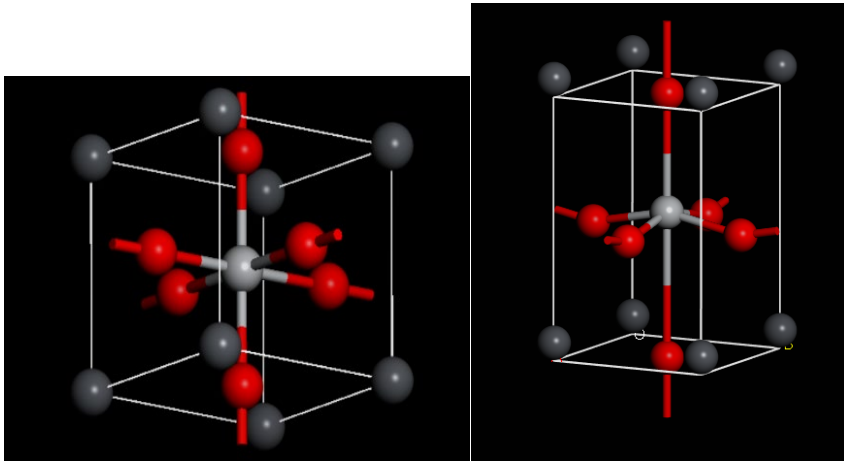

Figure 1: a) Cubic and b) Tetragonal structure of ATiO3 (A=Pb, Sn)

Table 1: Lattice Parameter and Volume for Cubic ATiO3 (A=Pb, Sn)

$ATiO_3$	Method	a (Å)	V (Å3)
$PbTiO_3$	LDA-CAPZ	3.892	58.9683
	GGA-PBE	3.973	62.7176
	GGA-PBEsol	3.929	60.6730
	Expt. [24]	3.960	62.0991
	Expt. [25]	4.049	66.3809
$SnTiO_3$	LDA-CAPZ	3.849	57.0611
	GGA-PBE	3.941	61.2004
	GGA-PBEsol	3.907	59.6346
	LDA-CAPZ [26]	3.850	57.0667
	GGA-PBE [27]	3.966	62.3818

Table 2: Lattice Parameter and Volume for Tetragonal ATiO3 (A=Pb, Sn)

$ATiO_3$	Method	a (Å)	c (Å)	c/a	V (Å3)
$PbTiO_3$	LDA-CAPZ	3.873	4.010	1.04	60.1888
	GGA-PBE	3.842	4.801	1.25	70.9006
	GGA-PBEsol	3.889	4.169	1.07	63.0891
	Expt. [24]	3.890	4.167	1.07	63.0555
	LDA-CAPZ [28]	3.860	3.840	0.99	57.2145
$SnTiO_3$	LDA-CAPZ	3.743	4.352	1.16	60.9917
	GGA-PBE	3.820	4.734	1.24	69.1056
	GGA-PBEsol	3.808	4.459	1.17	64.6546
	LDA-CAPZ [29]	3.800	4.090	1.08	59.0596
	PWPP [30]	3.812	3.800	0.99	55.2191

Band Structures and Density of States (DOS) of PTO and SnTO

The calculated electronic band structures of cubic PTO and SnTO at position of X (0.5, 0.0, 0.0), R (0.5, 0.5, 0.5), M (0.5, 0.5, 0.0) and G (0.0, 0.0, 0.0) using the GGA-PBE functional approximation in the Brillouin Zone is shown in Figure 2. For both PTO and SnTO, the most elevated valence band (VB) is ruled by the O-2p at X point, where it lies at the Fermi level. The most minimal conduction band (CB) is fundamentally overwhelmed by Ti-3d overlap with Pb-6p state at G-point. Five valence groups are mostly from the hybridisation of O-2p and Ti-3d orbitals beneath the Fermi level. These bands are very close and mixed. As calculated by using GGA-PBE functional, at X-G point, PTO has an indirect bandgap of 1.69 eV. In SnTO, the most astounding valence band (VB), which lies at the Fermi level (E_F), is commanded by the O 2p at X point that comparable with the PTO compound. The CB for SnTO happens at G point, which is fundamentally ruled by Ti 3d blended occupied together with Sn p-state. SnTO has an indirect bandgap of 1.64 eV, which is smaller 0.05 compared to PTO. This value is in agreement with the experimental data, which has an indirect bandgap of 2.361 eV by applying a 1.4 eV scissor operator [31]. It is emphatically foreseen that the SnTO could be a great possibility to be doped in any Pb compound because of their similitude in special lone pair ns^2 (n=5 for Sn and n=6 for Pb).

Electron dispersion in a vitality range could be portrayed by the density of state (DOS). Based on Figure 2, for the cubic structure, it indicates the CB area, which comprises predominantly of Ti 3d and Pb 6p nuclear orbitals with little commitments of O 2p and 2s states. The peak at Ti 3d shows a more grounded hybridisation between O 2p and Ti 3d when contrasted with O 2p and Pb 6s. As for SnTO, it can be seen that the VB of SnTO is just involved by electron O 2p and Sn 5s state. CB of SnTO is commanded by O 2p states that uncovered the presence of covalence association between cation Sn 5s (extraordinary solitary pair) and Ti 3d with O 2p states.

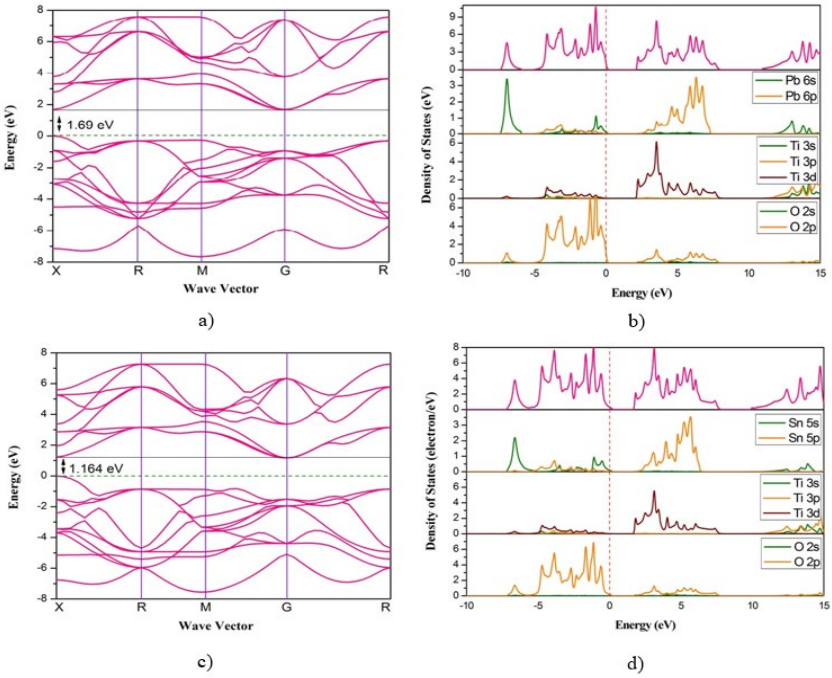

Figure 2: a) Bandgaps and b) DOS of Cubic $PbTiO_3$ and c) Bandgaps and d) DOS of Cubic $SnTiO_3$

Figure 3 displays the determined electronic band structures for tetragonal structures along the lines Z-A-M-G-Z-R-X-G at the high-symmetry Brillouin zone of PTO and SnTO. The Fermi level is set to be at 0 eV, and it shows that the most elevated valence band (VB) is commanded by the O 2p at X point for both PTO and SnTO while the conduction band (CB) Ti 3d and A-p state (A=Pb, Sn) fundamentally rule for PTO and SnTO happen at G point. It portrays the indirect bandgap of PTO is 1.703 eV at X-G point. As for SnTO, the least value calculation of the indirect bandgap is 1.164 eV an incentive for SnTO is lower contrasted than that of past research on the cubic stage SnTO with a bandgap of 1.64 eV. Nonetheless, the bandgap of tetragonal PTO (1.703 eV) is slightly higher than cubic PTO (1.69 eV) with a percentage deviation of 0.76%. For tetragonal material comprises of the $ATiO_3$ framework, a solid covalent bonding happens between Ti-O and that nature bonding is additionally established in PTO and SnTO as displayed in DOS.

Furthermore, high covalent bonding is produced between Pb-O and Sn-O when the cation with exceptional lone pair ns^2 states hybridised with the O 2p state. Be that as it may, the most noteworthy valence band (VB) in all materials, which lies at the Fermi level (EF), is principally credited to the O 2p states. While the conduction band (CB) is fundamentally overwhelmed by Ti 3d hybridise with the A (Pb, Sn) p-state for PTO and SnTO at the G point. This shows the strong covalent character displayed by A-O and Ti-O from the hybridisations between the lone pair (ns2) with O 2p and Ti-3d with O 2p individually.

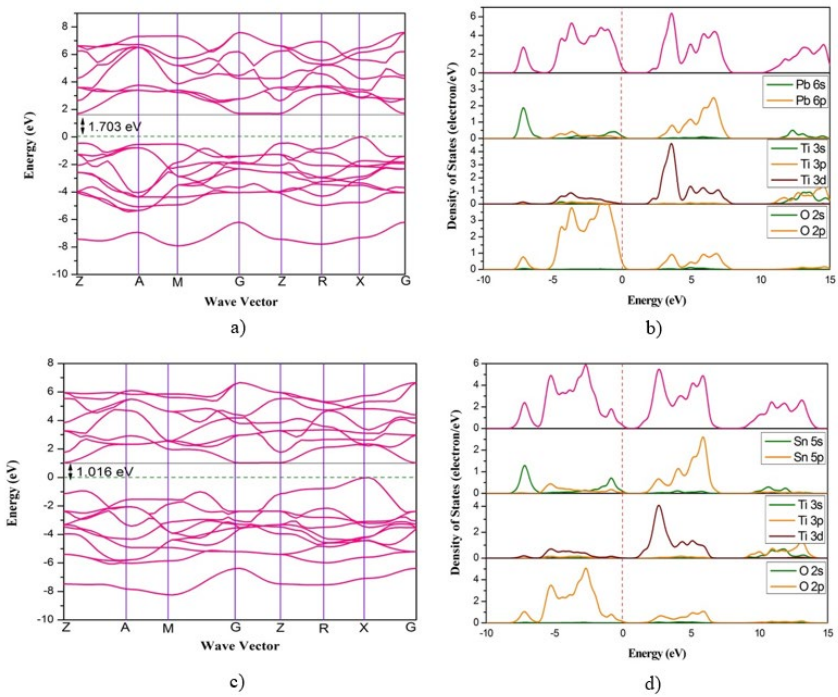

Figure 3: a) Band Gaps and b) DOS of Tetragonal $PbTiO_3$ and c) Band Gaps and d) DOS of Tetragonal $SnTiO_3$

CONCLUSION

In conclusion, the best functionality for the cubic structure is GGA-PBE, while GGA-PBEsol for the tetragonal PTO and SnTO, respectively. The electronic band structure for cubic $SnTiO_3$ is like $PbTiO_3$, which occurs at X-G point with a value of 1.164 eV and 1.69 eV, respectively. In any case, for the tetragonal structure of $PbTiO_3$ and $SnTiO_3$ demonstrates the bandgap at X-G point along the Brillouin zone with 1.703 eV and 1.016 eV individually. These outcomes are sensible and satisfactory, utilising an adjustment factor of 1.4 eV. The hybridisation of uncommon solitary pair (ns^2) with O 2p and hybridisation of Ti 3d with O 2p inferring solid covalent bonds were made.

ACKNOWLEDGEMENT

The authors would like to thank the Ministry of Higher Education (MOHE) Malaysia for funding this research under the FRGS grant 600-IRMI/FRGS 5/3 (121/2019) and Universiti Teknologi MARA (UiTM) for the facilities provided.

REFERENCES

[1] H. Zhang, C. Groh, Q. Zhang, W. Jo, G. Webber & J. Rodel, 2015. Large strain in relaxor/ferroelectric composite lead-free piezoceramics. *Advanced Electronic Materials, 1*(6), p. 1500018. https://doi.org/10.1002/aelm.201500018

[2] B. Hammer, L. B Hansen and J. K. Nørskov, 1999. Improved adsorption energetics within density-functional theory using revised Perdew-Burke-Ernzerhof functionals. *Physical Review B, 59*(11), p. 7413. https://doi.org/10.1103/PhysRevB.59.7413

[3] J. Hwang, Z. Feng, N. Charles, X. R. Wang, D. Lee, K. A. Stoerzinger, S. Muy, R. R. Rao, D. Lee, R. Jacobs, D. Morgan, & Y. Shao-Horn, 2019. Tuning perovskite oxides by strain: Electronic structure, properties, and functions in (electro)catalysis and ferroelectricity.

Materials Today, 31(xx), pp. 100–118. https://doi.org/10.1016/j.mattod.2019.03.014

[4] M. Tarnaoui, N. Zaim, M. Kerouad, & A. Zaim, 2020. Elastic, electronic and electrocaloric properties near room temperature in Mn-doped SnTiO3 from first-principles calculations. *Ceramics International, 46*(14), pp. 21995-22004. https://doi.org/10.1016/j.ceramint.2020.05.147

[5] M. S. Islam, 2019. Development and Characterization of Spark Plasma Sintered. [Master dissertation, Bangladesh University of Engineering and Technology]. Materials & Metallurgical Engineering (MME). Available at http://lib.buet.ac.bd:8080/xmlui/handle/123456789/5403

[6] H. M. Usama, 2018. Fabrication of High Quality Multiferroic BiFeO3 Based Thin Films Using Cost-Effective Processing Route. (Accession No. 146163023) [Master dissertation, Bangladesh University of Engineering and Technology]. Semantic Scholar Publishing. Available at https://www.semanticscholar.org/paper/Fabrication-of-high-quality-multiferroic-BiFeO3-Usama/61ecb74ea6de69f4a92d8dc2417ab3deaec7171f

[7] Y. Xu, D. Xue, Y. Zhou, T. Su, X. Ding, J. Sun, & E. K. H. Salje, 2019. Avalanche dynamics of ferroelectric phase transitions in BaTiO3 and 0.7Pb(Mg2?3Nb1?3)O3-0.3PbTiO3 single crystals. *Applied Physics Letters, 115*(2). https://doi.org/10.1063/1.5099212

[8] D. Maurya, M. Peddigari, M. G. Kang, L. D. Geng, N. Sharpes, V. Annapureddy, H. Palneedi, R. Sriramdas, Y. Yan, H. C. Song, Y. U. Wang, J. Ryu & S. Priya, 2018. Lead-free piezoelectric materials and composites for high power density energy harvesting. *Journal of Materials Research, 33*(16), pp. 2235–2263. https://doi.org/10.1557/jmr.2018.172

[9] H. Qiao, C. He, Z. Wang, X. Li, Y. Liu, and X. Long, 2017. Improved electrical properties of BaTiO3 modified BiScO3-PbTiO3 ceramics with high Curie temperature. *Ceramics International, 43*(14), pp. 11463-11468. https://doi.org/10.1016/j.ceramint.2017.06.021

[10] S. K. Porter, K. G. Scheckel, C. A. Impellitteri, & J. A. Ryan, 2004. Toxic metals in the environment: Thermodynamic considerations for possible immobilization strategies for Pb, Cd, As, and Hg. *Critical Reviews in Environmental Science and Technology, 34*(6), pp. 495–604. https://doi.org/10.1080/10643380490492412

[11] M. Rokosz, 2016. Metrology of the electrocaloric effect based on an infrared imaging technique. (Open Access) [Doctoral dissertation, Imperial College London]. Imperial College London Publishing. http://hdl.handle.net/10044/1/47999

[12] D. Vanderbilt, 1990. Soft self-consistent pseudopotentials in a generalized eigenvalue formalism. *Physical Review B, 41*(11), p. 7892. https://doi.org/10.1103/PhysRevB.41.7892

[13] S. Kuma, & M. M. Woldemariam, 2019. Structural, Electronic, Lattice Dynamic, and Elastic Properties of SnTiO3 and PbTiO3 Using Density Functional Theory. *Advances in Condensed Matter Physics, 2019.* https://doi.org/10.1155/2019/3176148

[14] Z. Zhen-Ye, B. Wang, W. Hai, & Y. Zhang, 2007. The first-principles study of ferroelectric behaviors of PbTiO3/SrTiO3 and BaTiO3/SrTiO3 superlattices. *Chinese Physics, 16*(6), p. 1780. https://doi.org/10.1088/1009-1963/16/6/051

[15] F. Cordero, F. Trequattrini, F. Craciun, H. T. Langhammer, D. A. B. Quiroga, & P. S. Silva, 2019. Probing ferroelectricity in highly conducting materials through their elastic response: Persistence of ferroelectricity in metallic BaTiO3-δ. *Physical Review B, 99*(6), pp. 1–11. https://doi.org/10.1103/PhysRevB.99.064106

[16] N. Kumada, Y. Yonesaki, T. Takei, N. Kinobura, and S. Wada, 2009. Preparation and crystal structure of a new tin titanate containing Sn2+; Sn2TiO4. *Materials Research Bulletin, 44*, pp. 1298-1300. https://doi.org/10.1016/j.materresbull.2008.12.017

[17] N. Noor, Q. Mahmood, M. Rashid, B. UlHaq, A. Laref, & S. Ahmad, 2018. Ab-initio study of thermodynamic stability, thermoelectric and

optical properties of perovskitesATiO 3 (A=Pb, Sn). *Journal of Solid State Chemistry, 263*, pp. 1-238. DOI: 10.1016/j.jssc.2018.04.017

[18] P. Hohenberg & W. Kohn, 1964. Density Functional Theory (DFT). Phys. *Rev, 136*, p. B864. https://doi.org/10.1103/PhysRev.136.B864

[19] M. Taib, M. Yaakob, O. Hassan, & M. Yahya, 2013. Structural, electronic, and lattice dynamics of PbTiO3, SnTiO3, and SnZrO3: A comparative first-principles study. *Integrated Ferroelectrics, 142*(1), pp. 119-127. https://doi.org/10.1080/10584587.2013.780528

[20] M. Taib, M. K. Yaakob, A. Chandra, A. K. Arof, & M. Z. A. Yahya, 2012. Effect of pressure on structural, electronic and elastic properties of cubic (Pm3m) SnTiO3 using first-principles calculation. *Advanced Materials Research, 501*, pp. 342-346. https://doi.org/10.4028/www.scientific.net/AMR.501.342

[21] R. Cuevas-Saavedra & V. N. Staroverov, 2016. Exact expressions for the Kohn–Sham exchange-correlation potential in terms of wave-function-based quantities. *Molecular Physics, 114*(7-8), pp. 1050-1058. https://doi.org/10.1080/00268976.2015.1131861

[22] R. I. Eglitis, 2019. Ab initio calculations of CaZrO3, BaZrO3, PbTiO3 and SrTiO3 (001), (011) and (111) surfaces as well as their (001) interfaces. *Integrated Ferroelectrics, 196*(1), pp. 7-15. DOI: 10.1080/10584587.2019.1591976

[23] M. F. M. Taib, M. K. Yaakob, O. H. Hassan, & M. Z. A. Yahya, 2013. Structural, Electronic, and Lattice Dynamics of PbTiO3, SnTiO3, and SnZrO3: A Comparative First-Principles Study. *Integrated Ferroelectrics, 142*(1), pp. 119-127. DOI: 10.1080/10584587.2013.780528

[24] L. Wang, P. Yuan, F. Wang, E. J. Liang, Q. Sun, Z. X. Guo, & Y. Jia, 2014. First-principles study of tetragonal PbTiO3: Phonon and thermal expansion. *Materials Research Bulletin, 49*, pp. 509-513. http://dx.doi.org/10.1016/j.materresbull.2013.08.075

[25] M. Sepliarsky, Z. Wu, A. Asthagiri, & R. Cohen, 2004. Atomistic model potential for PbTiO3 and PMN by fitting first-principles results. *Ferroelectrics, 301*(1), pp. 55-59. https://doi.org/10.1080/00150190490454882

[26] R. Z. Zhang, D. W. Wang, F. Li, H. J. Ye, X. Y., Wei, & Z. Xu, 2013. High performance lead-free ferroelectric A TiO3/SnTiO3 superlattices. *Applied Physics Letters, 103*(6), p. 062905. https://doi.org/10.1063/1.4818271

[27] H. Ye, R. Zhang, D. Wang, Y. Cui, J. Wei, C. Wang, Z. Xu, S. Qu, & X. Wei, 2013. First-Principles Calculation Of Lead-Free Perovskite SnTiO3. *International Journal of Modern Physics B, 27*(24), p. 1350144. https://doi.org/10.1142/S0217979213501440

[28] T. Shimada, S. Tomoda, & T. Kitamura, 2010. First-principles study on ferroelectricity at PbTiO3 surface steps. *Journal of Physics: Condensed Matter, 22*(35), p. 355901. DOI: 10.1088/0953-8984/22/35/355901

[29] Y. Konishi, M. Ohsawa, Y. Yonezawa, Y. Tanimura, T. Chikyow, T. Wakisaka, & K. Sasata, 2002. Possible ferroelectricity in SnTiO3 by first-principles calculations. MRS Online Proceedings Library Archive, p. 748. DOI: 10.1557/PROC-748-U3.13

[30] Y. Uratani, T. Shishidou, & T. Oguchi, 2008. First-principles study of lead-free piezoelectric SnTiO3. *Japanese Journal of Applied Physics, 47*(9S), p. 7735. DOI: 10.1143/JJAP.47.7735

[31] X. S. Xu, T. V. Brinzari, S. Lee, Y. H. Chu, L. W. Martin, A. Kumar, S. McGill, R. C. Rai, R. Ramesh, V. Gopalan, S. W. Cheong, J. L. Musfeldt, 2009. Optical properties and magnetochromism in multiferroic BiFeO3. *Physical Review B, 79*(13), p. 134425. DOI: 10.1103/PhysRevB.79.134425